Journal of Power Sources 239 (2013) 94–102

Contents lists available at SciVerse ScienceDirect

Journal of Power Sources

journal homepage: www.elsevier.com/locate/jpowsour

Effect of nitrogen-doped acetylene carbon black supported Pd nanocatalyst on formic acid electrooxidation

Jinfa Chang [a,b], Xiujuan Sun [a], Ligang Feng [a], Wei Xing [a,*], Xiujuan Qin [b], Guangjie Shao [b,**]

[a] State Key Laboratory of Electroanalytical Chemistry, Laboratory of Advanced Power Sources, Changchun Institute of Applied Chemistry, 5625 Renmin Street, Changchun 130022, PR China
[b] State Key Laboratory of Metastable Materials Science and Technology, Yanshan University, Qinhuangdao 066004, PR China

HIGHLIGHTS

- Palladium nanoparticles supported on the N-doped carbon materials used for FAEO.
- Pd/N-C-900 catalyst shows the best catalytic activity and stability for FAEO.
- Syngenetic effect of catalyst and support proposed for the catalytic process.

ARTICLE INFO

Article history:
Received 14 January 2013
Received in revised form
12 March 2013
Accepted 15 March 2013
Available online 26 March 2013

Keywords:
Direct formic acid fuel cells
Electrooxidation
Palladium nanoparticles
Nitrogen-doped
Synergetic effect

ABSTRACT

Nitrogen-doped acetylene carbon black (N-C) is prepared by annealing acetylene carbon black and melamine under the protection of N_2 at different temperatures. The resultant N-C materials are used as the support of Pd catalyst (Pd/N-C) for formic acid electrooxidation (FAEO). The catalytic activity of the Pd/N-C catalyst towards FAEO is evaluated by cyclic voltammetry, CO_{ad} stripping voltammetry and chronoamperometry. The results show that when the heat-treatment temperature of support is 900 °C, the corresponding catalyst, Pd/N-C-900, generate 2.84-fold and 0.96-fold higher activity than homemade and commercial Pd/C catalysts in 0.5 M H_2SO_4 and 0.5 M HCOOH solution. The CO_{ad} stripping voltammetry results demonstrate that Pd/N-C-900 has much better resistance to CO poisoning. Moreover, the effect of formic acid concentration and the temperature on the Pd/N-C catalysts are also explored, which confirms the really enhanced performances for FAEO. It is founded that the doping of nitrogen results an increase in the performance for FAEO due to the improved Pd nanoparticles (Pd NPs) dispersion and the modified electronic effect. The results indicate that the Pd/N-C catalyst has great application prospect as a high-performance anode catalyst for direct formic acid fuel cells (DFAFCs).

1. Introduction

Driven by the demand of clean and high-efficiency energy conversion devices, direct formic acid fuel cells (DFAFCs) have received considerable attention due to the formic acid possessing fast oxidation kinetics, less toxicity, lower crossover rate through Nafion membrane than methanol [1–6]. More importantly, formic acid is environment-friendly and non-toxic to human beings [7,8]. However, the anode catalysts still limit the commercial development of fuel cell. It is well known that Pt is a good catalyst for formic acid electrooxidation (FAEO), while the oxidation of formic acid on Pt is hindered by indirect mechanism [9]. On the other hand, the high price of platinum is also a setback to its use for commercial applications. In an effort to reduce indirect mechanism and the cost of catalysts used for FAEO, attention has been shifted to non-Pt catalysts such as Pd. Results show that Pd and Pd/C catalysts have much higher catalytic activity for FAEO than Pt-based catalysts because they can overcome the CO poisoning [10].

Although palladium-based catalysts have better catalytic activity than platinum-based, it is important to note that Pd deactivates during formic acid oxidation [8,11–14]. Blair et al. [15] studied the long-term stability of Pt, Pd, and various Pd–Pt catalysts by chronopotentiometry and found that the Pd activity, although initially substantially higher compared to Pd–Pt alloys, falls below the activity of Pd–Pt and Pt within about 6 h. Li and Hsing [13] reported the formic acid oxidation current on Pd decreased by a factor of 10 over a 30 min period. The Pd deactivation during formic acid oxidation is not well understood at present and more studies are required to elucidate its mechanism. According to Arenz et al. [11],

* Corresponding author. Tel.: +86 431 85262223; fax: +86 431 85685653.
** Corresponding author. Tel./fax: 86 335 8061569.
E-mail addresses: xingwei@ciac.jl.cn (W. Xing), shaogj@ysu.edu.cn (G. Shao).

0378-7753/$ – see front matter © 2013 Elsevier B.V. All rights reserved.
http://dx.doi.org/10.1016/j.jpowsour.2013.03.066

Pd deactivation could be due to poisoning of the formic acid oxidation active sites (e.g., specific crystal planes) by 'spectator' species such as H_{ad} and OH_{ad}, and anions from the supporting electrolyte (e.g., SO_4^{2-}). Although the palladium as a catalyst for formic acid electrooxidation has been widely studied, the poor catalytic activity and stability at the anode for FAEO reaction and high cost of noble metal catalysts are still the major challenges for the practical development of DFAFCs [7,12,16].

On the other hand, in order to develop the efficient electrocatalysts, great attention has been directed to the novel effective catalyst supports, on which the metal catalysts are dispersed as they play a crucial role in improving the catalytic activity. They can alter the electronic character and the geometry of the catalyst particles dispersed on their surface [17,18]. Carbon black (e.g. Vulcan XC-72) is the commonly used support material, while the surface area is low leading to low catalysts utilization. Meanwhile, mesoporous carbon, carbon nanotubes (CNTs), graphene, graphene oxide (GO), graphite nanofibers (GNFs) and graphitic carbon nanocoils (GCNC) and so on are used as carbon supports. While most of the above carbon supports are expensive or need complicated technology or serious conditions during preparation. Hence, tremendous efforts have been devoted to searching for new, cheap and easy-prepared catalyst supports to achieve good dispersion, utilization, activity and stability. Recent research demonstrated that carbon-based support materials can be doped by nitrogen to create strong, beneficial catalyst–support interactions which substantially enhance the catalyst activity and stability [19–23]. Xiong [24] and his co-workers used nitrogen-doped graphene supporting Pt NPs (Pt/N-G) as a catalyst for methanol oxidation reaction (MOR), which exhibited higher electrocatalytic activity towards MOR. Zhao et al. [25] used Pt/TiO_2@N-doped C nanocomposite for MOR, the catalyst they prepared exhibited higher activity, stability and much better resistance to CO poisoning than commercial Pt/C catalyst. Bae et al. [26] prepared nitrogen-containing carbon materials by pyrolysis of acetonitrile on carbon black and the resultant N-C was used as a support for Pt catalyst (Pt/N-C), which exhibited increased activity and stability in electrochemical hydrogen oxidation. Yoon et al. [27] studied Pd nanoparticles deposited on nitrogen-doped magnetic carbon nanoparticles (Pd/N-MCNPs), the results displayed high catalytic activity for coupling reactions. However, the Pd catalysts supported on nitrogen doped carbon for FAEO were seldom reported.

In this paper, in order to investigate the effect of nitrogen-doped acetylene carbon black supported Pd nanocatalyst on FAEO, a series of N-C supports were successfully prepared by annealing acetylene carbon black and melamine at different temperatures. The resultant N-C materials were used as conductive supports of Pd catalyst (Pd/N-C) for FAEO. The catalysts were prepared through a facile microwave-assisted polyol reduction process, and the as-prepared catalysts exhibited much better tolerance of CO poisoning, much higher catalytic activity and stability for FAEO than the homemade and commercial catalysts.

2. Experimental

2.1. Catalyst preparation

2.1.1. Preparation of nitrogen-doped acetylene carbon black support

Firstly, 0.14 g of melamine and 0.35 g acetylene carbon black (denoted as C) were homogenized into fine powders using a mortar and pestle. After that, the solid mixture was transferred to a tubular oven at 900 °C under the protection of N_2 for 1 h (the temperature was ramped at a rate of 5 °C min^{-1} to the final treatment and the flow of N_2 was 80 cc min^{-1}) to obtain the stable nitrogen doped acetylene carbon black support (denoted as N-C-900). Other heat-treatment temperatures were also applied to investigate the effects of heat-treatment temperature and they were referred to as N-C-*T* ($T = 700$, 800 and 1000 °C). It should be noted that all solutions in our work were prepared using Millipore-MiliQ water (resistivity: $\rho \geq 18$ MΩ cm^{-1}) and the reagents used were analytical-grade.

2.1.2. Preparation of palladium catalyst supported on N-C-T

The palladium catalysts supported on nitrogen doped acetylene carbon black with 20 wt.% Pd were prepared according to previous work [28]. Briefly, 80 mg of N-C-*T* support was ultrasonically dispersed in 50 ml of ethylene glycol to form a uniform suspension. Under stirring, a certain amount of H_2PdCl_4 solution (contain 20 mg Pd) was added to the suspension, and the pH of the suspension was adjusted to approximately 11 with 1 M NaOH solution (dissolved in ethylene glycol). Then the suspension was placed and exposed in the middle of a microwave oven (LGMG-5021MW1, 2450 MHz) with 700 W with 45 s on and 15 s off cycle for three times and cooled to room temperature naturally. At last, the suspension was filtered, washed and dried overnight at 80 °C in a vacuum oven to obtain the Pd/N-C-*T* catalyst. The palladium catalyst supported on acetylene carbon black without nitrogen-doped (denoted as Pd/C) was prepared by the same method for comparison nitrogen doping effect. A commercial Pd/C catalyst (denoted as Pd/C-C, Sigma–Aldrich 407305-10G) was used for comparison as a baseline catalyst. In this work, most of electrochemical data were normalized to the mass of Pd to compare the performance and intrinsic activity of different catalysts.

2.2. Electrochemical measurements

All the electrochemical measurements were performed with an EG & G PARC potentiostat/galvanostat (Model 273A Princeton Applied Research Co., USA) and a conventional three compartment electrochemical cell. A Pt foil and a saturated calomel electrode (SCE) were used as the counter and the reference electrodes, respectively. All potentials were referenced to SCE. The working electrode was prepared as follows. First, 5 mg of the catalyst was dispersed ultrasonically in 1000 μL of the alcohol solution containing 100 μL Nafion solution (5 wt.%, Aldrich Co., USA). Second, 10 μL of the above solution was pipetted and spread on a mirror-finished glassy carbon electrode with 4 mm diameter. At last, it was dried at room temperature for 30 min. The glassy carbon electrode was polished with alumina slurry of 0.5 and 0.03 μm successively.

All electrochemical measurements were carried out in a 0.5 M H_2SO_4 solution with or without HCOOH deaerated by pure N_2 for at least 20 min prior to any measurements. For the electrooxidation of formic acid, the scan potential range was from −0.2 to +1.0 V. The CO_{ad} stripping voltammograms were measured in a 0.5 M H_2SO_4 solution. CO was purged into the 0.5 M H_2SO_4 solution for 15 min to allow the complete adsorption of CO onto the catalyst when the working electrode was kept at 0.2 V, and excess CO in the electrolyte was purged out with N_2 for 30 min. All the measurements were carried out at room temperature, unless otherwise noted; and the stable results were reported. The surface area of Pd metal was estimated assuming that the coulombic charge necessary for oxidation of a monolayer of linearly adsorbed H was 210 μC cm^{-2} [29] while CO was 420 μC cm^{-2} [30,31].

2.3. Physical characterization

The composition of the catalysts was analyzed by energy dispersive X-ray (EDX) analysis on a scanning electron microscope operating at 20 kV (JEOL JAX-840), X-ray diffraction (XRD) measurements were performed with a PW-1700 diffractometer using a

Cu K_α (λ = 1.5405 Å) radiation source (Philips Co.), the obtained XRD patterns were analyzed with Jade 5.0 software to remove the background radiation, X-ray photoelectron spectroscopy (XPS) measurements were carried out on Mg K_α radiation source (Kratos XSAM-800 spectrometer), the size and morphology of the catalysts were measured by transmission electron microscope (TEM) operating at 200 kV (Philips TECNAI G2).

3. Results and discussion

3.1. Electrochemical analysis

Fig. 1 shows cyclic voltammograms (CVs) of the Pd/C-C, Pd/C, Pd/N-C-*T* catalysts in 0.5 M H_2SO_4 solution at the scan rate of 50 mV s^{-1}. It is clear that all catalysts showed the expected behaviour of Pd electrode in H_2SO_4 solution with characteristic and well defined hydrogen adsorption/desorption (H_{ad}) peaks around −0.05 V and Pd oxide reduction peak in the reverse scan at ca. 0.45 V. All these features are typical for Pd catalysts in H_2SO_4 solution and agree well with the reported data [9,32–35]. Obviously, the commercial Pd/C-C catalyst showed higher double layer capacitance than Pd/C and Pd/N-C-*T* catalysts, while all the catalysts with nitrogen-doped have a larger peak area than the Pd/C catalyst according to the area of the H_{ad} peaks of six catalysts, indicating that the catalysts by nitrogen doping possess a larger electrochemical surface area (ECSA). The detailed data are shown in Table 1. The ECSA of the catalysts integration from the H_{ad} showed an order of Pd/C < Pd/C-C < Pd/N-C-1000 < Pd/N-C-800 < Pd/N-C-700 < Pd/N-C-900.

CO_{ad} stripping, as a structure-sensitive reaction, was adopted to evaluate the difference in the resistance to CO and ECSA of different catalysts. CO_{ad} stripping voltammograms for different catalysts in 0.5 M H_2SO_4 solution with a scan rate of 50 mV s^{-1} are shown in Fig. 2. The ECSA of the six catalysts by integration of the CO_{ad} stripping peak are shown in Table 1, which showed an order of Pd/C < Pd/N-C-1000 < Pd/C-C < Pd/N-C-700 < Pd/N-C-800 < Pd/N-C-900. Typically, the ECSA of Pd/N-C-900 catalyst were 82.70 $m^2\ g^{-1}$, which has increased approximately 32% and 46% compared to the Pd/C-C (62.63 $m^2\ g^{-1}$) and Pd/C (56.62 $m^2\ g^{-1}$) catalysts. The peak potential (V) for CO_{ad} stripping for the six catalysts is also shown in Table 1, the Pd/N-C-900, Pd/C-C and Pd/C catalysts showed primary CO_{ad} stripping peaks located at 0.666, 0.687 and 0.760 V, respectively. The oxidation peak and the onset potential for CO_{ad} oxidation for Pd/N-C-T catalysts were shifted negatively compare to Pd/C catalyst, indicating that the addition of nitrogen in carbon support was helpful in weakening the CO adsorptive bond on the Pd active sites. While when the heat-treatment temperature was 1000 °C, the corresponding catalyst, Pd/N-C-1000, have a similar CO_{ad} stripping peak potential compared to Pd/C, indicating that these two catalysts have a similar tolerance of CO poisoning.

Table 1
ECSA integration from the H_{ad} and CO_{ad} stripping experiment and peak potential for CO_{ad} stripping for the six catalysts in 0.5 M H_2SO_4 solution with a scan rate of 50 mV s^{-1}.

Sample	Pd/C-C	Pd/C	Pd/N-C-700	Pd/N-C-800	Pd/N-C-900	Pd/N-C-1000
ECSA[a] ($m^2\ g^{-1}$)	47.78	43.20	59.07	50.26	80.88	48.12
ECSA[b] ($m^2\ g^{-1}$)	62.63	56.62	64.11	68.00	82.70	60.61
Peak potential (V)	0.687	0.760	0.706	0.697	0.666	0.759

[a] The ECSA of the catalysts integration from the H_{ad} experiment.
[b] The ECSA of the catalysts integration from the CO_{ad} stripping experiment.

Fig. 3 displays the CVs of different catalysts in 0.5 M H_2SO_4 + 0.5 M HCOOH solution with a scan rate of 50 mV s^{-1}. The peak current density (mA mg_{Pd}^{-1}) and the corresponding peak potential (V) of six catalysts are shown in Table 2. Clearly, the peak current density of the catalysts showed an order of Pd/C < Pd/N-C-1000 < Pd/C-C < Pd/N-C-700 < Pd/N-C-800 < Pd/N-C-900. Typically, the peak current density of Pd/N-C-900 catalyst was 1202 mA mg_{Pd}^{-1}, which was about 2.84 times higher than the Pd/C catalyst (313 mA mg_{Pd}^{-1}) and even about 0.96 times higher than the commercial Pd/C-C catalyst (613 mA mg^{-1} Pd). The peak potential of the catalysts showed an order of Pd/C-C < Pd/N-C-900 < Pd/N-C-800 < Pd/N-C-700 < Pd/N-C-1000 ≈ Pd/C. Here, the oxidation peak potential of Pd/N-C-900 catalyst shifted 46 mV towards negative potential compared with the Pd/C catalyst. All the catalysts doped with nitrogen display a better performance than undoped-nitrogen catalyst. From this aspect, it was thought that the FAEO on the Pd catalysts doped with nitrogen were much easier than undoped-nitrogen catalyst. While when the heat-treatment temperature was 1000 °C, the catalytic activity for formic acid was sharply reduced, consistent with the above study of H_{ad} and CO_{ad} stripping measurement. On the other hand, the peak potential of Pd/N-C-1000 and Pd/C was very close,

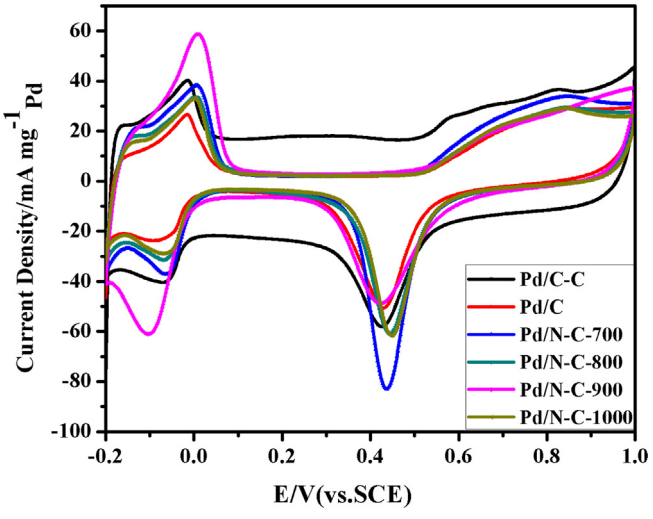

Fig. 1. CVs of different catalysts in 0.5 M H_2SO_4 solutions with a scan rate of 50 mV s^{-1}.

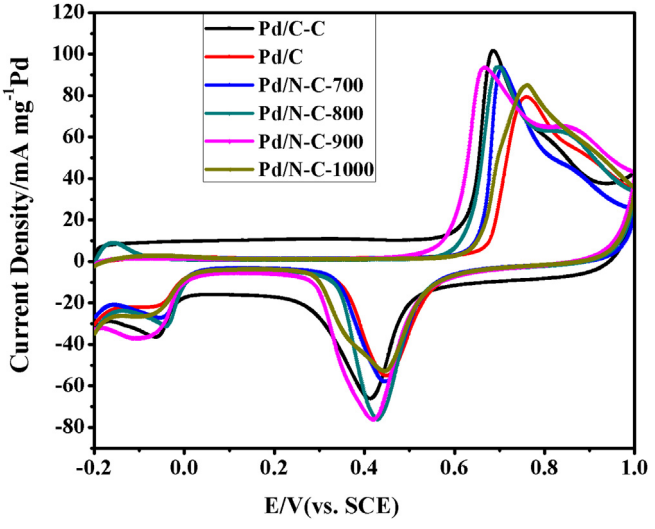

Fig. 2. CO_{ad} stripping voltammograms for different catalysts in 0.5 M H_2SO_4 solution with a scan rate of 50 mV s^{-1}.

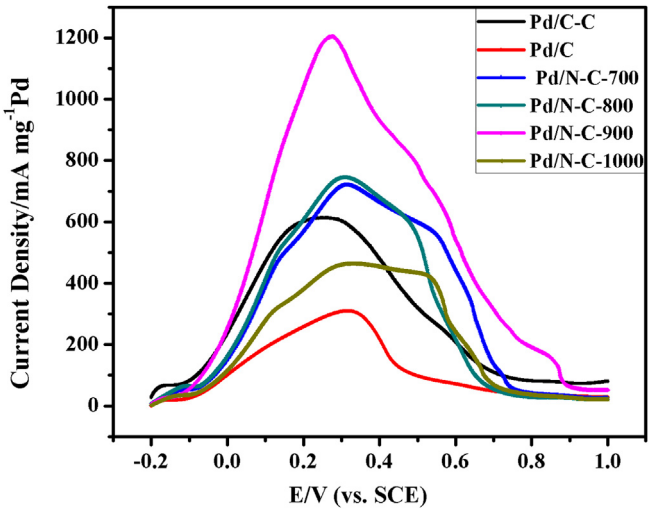

Fig. 3. CVs of different catalysts in 0.5 M H_2SO_4 + 0.5 M HCOOH solution with a scan rate of 50 mV s^{-1} at 25 °C.

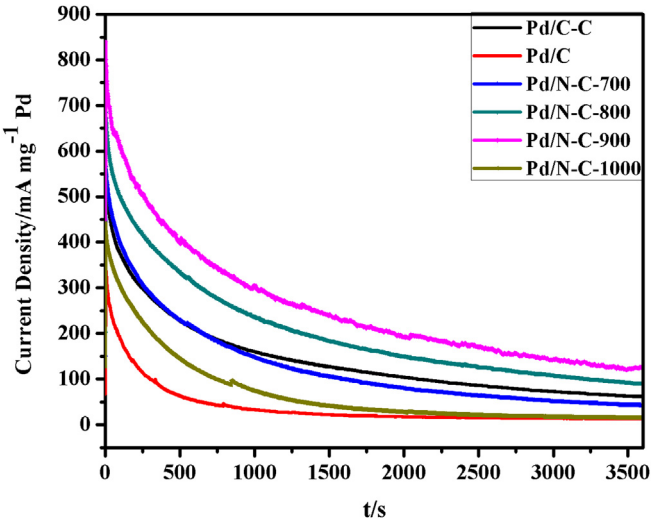

Fig. 4. Chronoamperometric curves of different catalysts in 0.5 M H_2SO_4 + 0.5 M HCOOH solution at 0.2 V at 25 °C.

which was consistent with CO_{ad} test. Considering that the tremendous increase of peak current density and the negative shift peak potential of Pd/N-C-900 catalyst compared with the Pd/C catalyst, the performance increase cannot be simply attributed to the increased ECSA as the ECSA of Pd/N-C-900 catalyst was 1.87-fold and 1.46-fold than the Pd/C catalyst from the measurement of H_{ad} and CO_{ad}. The current increase and negative shift of peak potential should be more reasonably attributed to the existence of nitrogen in the carbon support of catalysts.

Chronoamperometric curves were used to compare the electrochemical stabilities of the as-prepared catalysts for FAEO. Fig. 4 shows the chronoamperometric curves of the six catalysts in 0.5 M H_2SO_4 containing 0.5 M HCOOH solution at 0.2 V for 3600 s. The results were obtained after the above electrochemical test. Clearly, the current density of Pd/N-C-900 catalyst for FAEO remains higher than the other catalysts and all the curves reach a steady state after about 3000 s. Typically, the current density at 1000 s was about 301, 160 and 33 mA mg_{Pd}^{-1} for Pd/N-C-900, Pd/C-C and Pd/C catalysts, respectively. Even after 3600 s, the current density of Pd/N-C-900 catalyst was still 123 mA mg_{Pd}^{-1}, which was approximately one times higher than Pd/C-C catalyst (61 mA mg_{Pd}^{-1}) and 5.5 times higher than Pd/C catalyst (16 mA mg_{Pd}^{-1}). This result indicated that the Pd/N-C-900 catalyst has a much better catalytic activity and stability than homemade and commercial Pd/C catalyst for FAEO. On the other hand, this result was in agreement with the result of H_{ad}, CO_{ad} stripping and CVs of FAEO, which suggested that the existence of nitrogen in the support of catalyst could increase the electrocatalytic activity and stability.

In order to investigate the effect of formic acid concentration on Pd/N-C catalysts for FAEO, Fig. 5 shows the CVs of the catalysts in 5 M or 10 M HCOOH and 0.5 M H_2SO_4 at room temperature to compare the catalytic activity. The peak current density (mA mg_{Pd}^{-1}) and the corresponding peak potential (V) of six catalysts in detail were also listed in Table 2. It can be seen that the Pd/N-C-900 catalyst in 5 M or 10 M HCOOH has the largest peak current density compared with other Pd/N-C catalysts even with the commercial Pd/C-C catalyst in the same formic acid concentration. While for the same catalyst, the peak current density is not multiple increases with the increase of the formic acid concentration. For example, the peak current density of the commercial Pd/C-C catalyst in 5 M HCOOH was 1425 mA mg_{Pd}^{-1}, while in 10 M HCOOH solution the value was 1770 mA mg_{Pd}^{-1}, which is due to the limitation of the mass transfer resistance. The oxidation peak potential of Pd/N-C-900 catalyst in 0.5 M H_2SO_4 + 5 (10) M HCOOH solution shifted 129 (102) mV towards negative potential compared with the Pd/C catalyst, which is consistent with the data in 0.5 M H_2SO_4 + 0.5 M HCOOH solution.

The performances of all the catalysts in 0.5 M H_2SO_4 + 0.5 M HCOOH solution at 40 °C and 60 °C are also compared in Fig. 6, and the details of the peak current density (mA mg_{Pd}^{-1}) and the corresponding peak potential (V) of six catalysts are also shown in Table 2. It can be seen that the peak current density of all the

Table 2
The peak current density and the corresponding peak potential for FAEO of the six catalysts in 0.5 M H_2SO_4 at 50 mV s^{-1} in different test conditions.

Catalysts test condition		Pd/C-C	Pd/C	Pd/N-C-700	Pd/N-C-800	Pd/N-C-900	Pd/N-C-1000
0.5 M HCOOH	Peak current (mA mg_{Pd}^{-1})	613	313	721	745	1202	462
25 °C	Peak potential (V)	0.234	0.317	0.314	0.311	0.271	0.317
5 M HCOOH	Peak current (mA mg_{Pd}^{-1})	1425	1160	1490	1542	2471	1100
25 °C	Peak potential (V)	0.274	0.392	0.352	0.340	0.263	0.369
10 M HCOOH	Peak current (mA mg_{Pd}^{-1})	1770	1602	1709	1808	2491	758
25 °C	Peak potential (V)	0.303	0.360	0.380	0.335	0.258	0.332
0.5 M HCOOH	Peak current (mA mg_{Pd}^{-1})	1263	1137	1646	1791	2173	1177
40 °C	Peak potential (V)	0.315	0.360	0.386	0.300	0.297	0.335
0.5 M HCOOH	Peak current (mA mg_{Pd}^{-1})	2458	1819	2526	2907	3874	1870
60 °C	Peak potential (V)	0.270	0.356	0.390	0.321	0.310	0.356

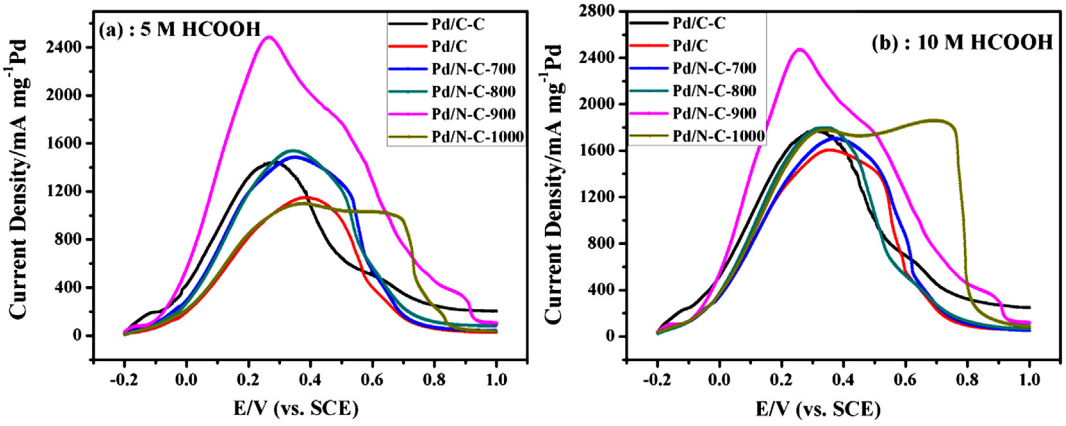

Fig. 5. CVs of different catalysts in 0.5 M H_2SO_4 + 5 M HCOOH solution (a) and 0.5 M H_2SO_4 + 10 M HCOOH solution (b) with a scan rate of 50 mV s^{-1}.

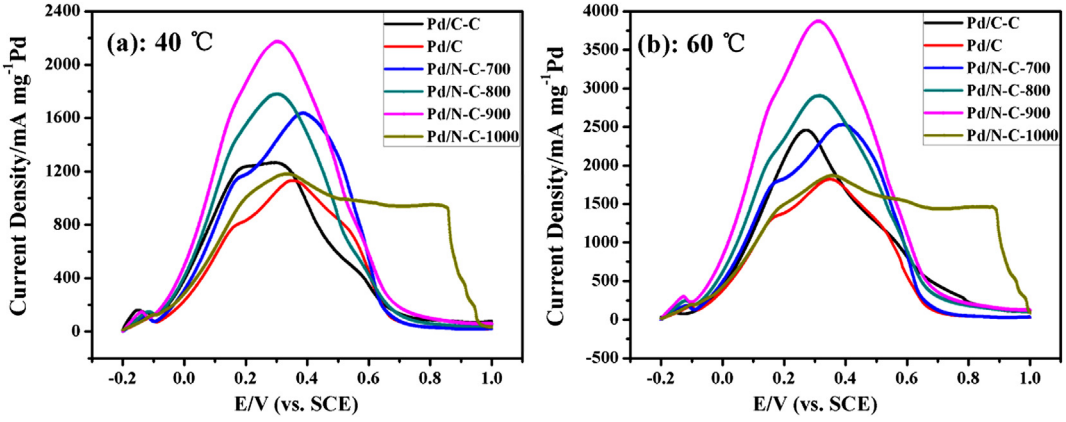

Fig. 6. CVs of different catalysts in 0.5 M H_2SO_4 + 0.5 M HCOOH solution at 40 °C (a) and 60 °C (b) with a scan rate of 50 mV s^{-1}.

catalysts increased with the increase of the temperature. Moreover, the oxidation peak potential of Pd/N-C-900 catalyst negatively shifted compared with the Pd/C catalyst. The above results demonstrated that all the catalysts doped with nitrogen display a better performance than the undoped-nitrogen catalyst and the Pd/N-C-900 catalyst still has the best performance, which is consistent with the data in 0.5 M H_2SO_4 + 0.5 M HCOOH solution performed at 25 °C.

From the above electrochemical analysis, it could be concluded that the optimal heat-treatment temperature for N-C support temperature was 900 °C. To further study the reasons for the enhanced performance of the catalyst, physical characterization for Pd/C-C, Pd/C and Pd/N-C-900 were evaluated as follows.

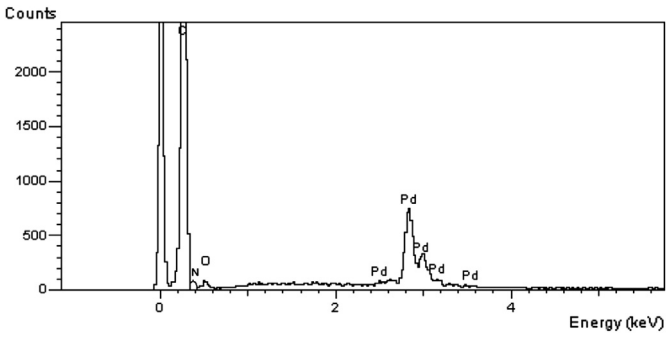

Fig. 7. EDX spectrum for the Pd/N-C-900 catalyst.

3.2. Physical characterization

Fig. 7 shows a typical EDX spectrum for the Pd/N-C-900 catalyst. The composition of the Pd/N-C-900 catalyst consists of C (70.92 wt.%), N (0.72 wt.%), O (8.52 wt.%) and Pd (19.54 wt.%), respectively. The result indicated that nitrogen was successfully doped in the Pd/N-C-900 catalyst and the atomic ratio of C, N, O and

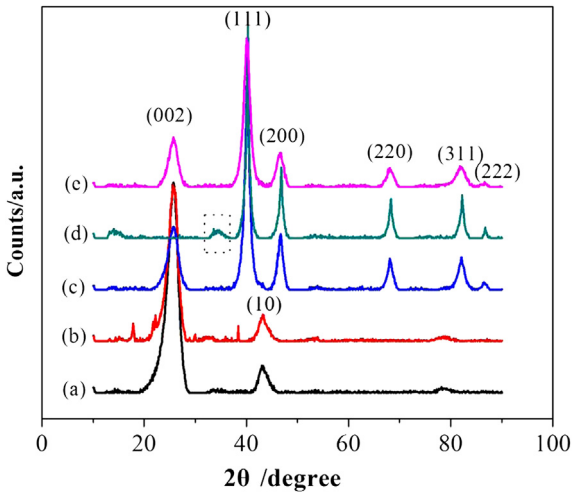

Fig. 8. XRD patterns for the supports acetylene carbon black (a), N-C-900 (b) and catalysts Pd/C (c), Pd/C-C (d) and Pd/N-C-900 (e).

Pd was 0.887:0.008:0.075:0.030. The ratio of C determined by EDX was generally a little higher than expected, while the Pd ratio was a little lower. Since these discrepancies were within the normal uncertainty of EDX, the results indicate that there were no significant deviations from the expected compositions.

The typical XRD patterns of C, N-C-900 support and the catalysts were shown in Fig. 8. The peak observed at about 25.8° in Fig. 8(a), (b), (c) and (e) was assigned to the (002) reflection of the hexagonal structure of graphite, and the peak at around 43.1° for the C and N-C-900 support materials can be assigned to the (10) diffractions of the graphitic framework [36]. The disappearance of 43.1° in Fig. 8(c) and (e) may be owing to the strong diffraction peak of Pd, which covers up the (10) diffractions of the graphitic framework. There was no diffraction peak at about 25.8° in Fig. 8(d), which could be attributed to the existence of amorphous carbon in commercial Pd/C-C catalyst. In comparison to original C support, the peaks observed at about 17.9°, 22.2° and 38.3° in N-C-900 support were found in Fig. 8(b); on the other hand, the XRD patterns of N-C-900 support were hairy while the C support without nitrogen-doped, Fig. 8(a) were smooth, all these results were attributed to the function of doping nitrogen. The three Pd-based catalysts exhibited five characteristic diffraction peaks observed at about 40.1°, 46.7°, 68.1°, 81.8°, 86.8° correspond to the (111), (200), (220), (311) and (222) crystal faces of Pd, respectively [37]. It should be noted that the XRD patterns for the Pd/C-C catalyst also display a diffraction peak at approximately 34.2° in Fig. 8(d), which could be due to the

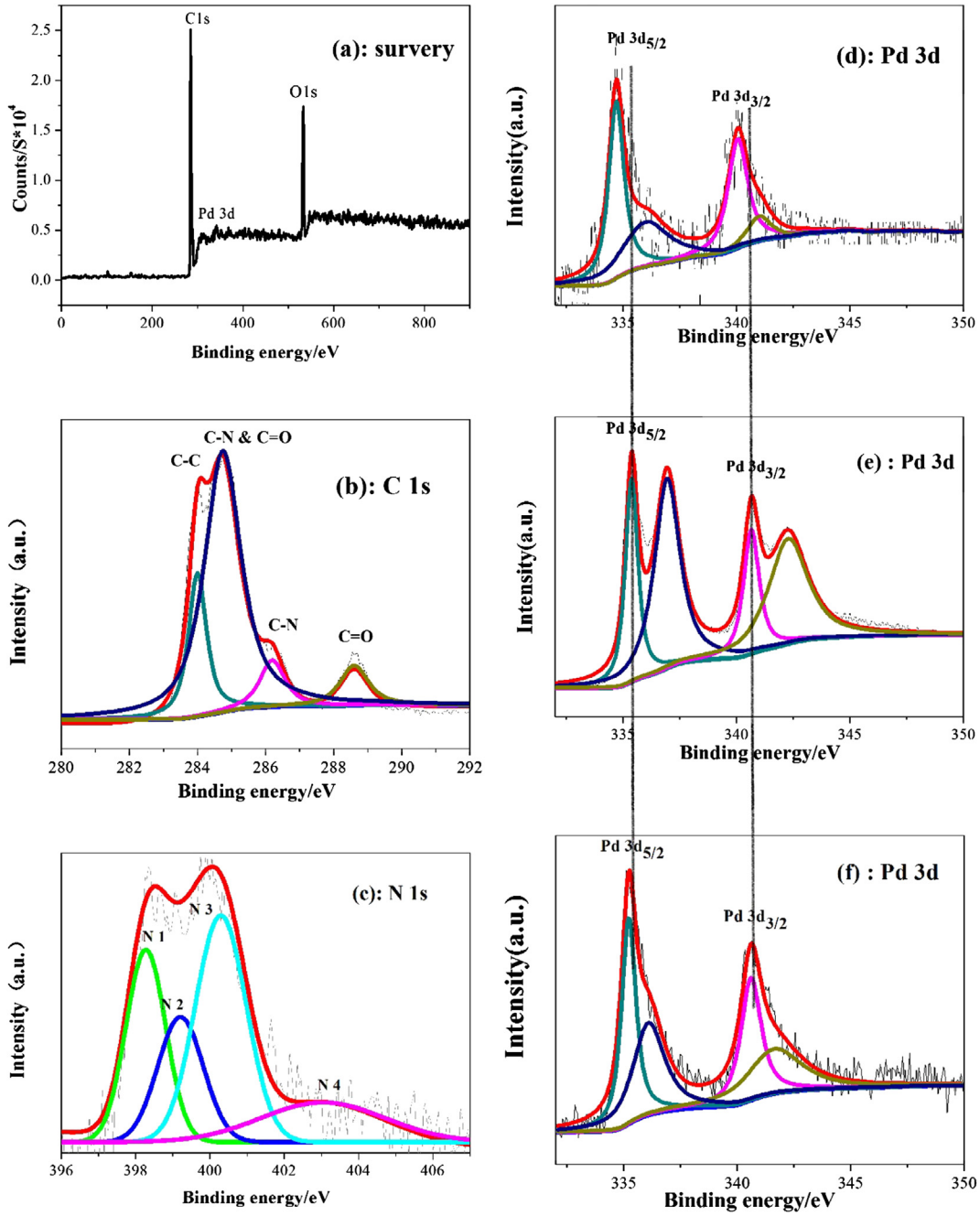

Fig. 9. XPS spectra of Pd/N-C-900, Pd/C-C and Pd/C: survey spectra of Pd/N-C-900 catalyst (a), high-resolution spectra of C 1s (b), N 1s (c) of Pd/N-C-900 catalyst; high-resolution spectra of Pd 3d for Pd/N-C-900 (d), Pd/C-C (e) and Pd/C (f) catalyst.

presence of Pd oxides/hydrous oxides [16]. The diffraction peaks of the Pd/N-C-900 catalyst were broader than those of the Pd/C and Pd/C-C catalysts, indicating that the average size of the Pd particles in the Pd/N-C-900 catalyst was smaller than that of the Pd/C and Pd/C-C catalysts and the relative crystallinity of the Pd/N-C-900 catalyst was lower than the other two catalysts. The average particle size, calculated from the Pd (220) peak according to the Scherrer formulae [38] for the Pd/C, Pd/C-C and Pd/N-C-900 catalysts was 4.3 nm, 4.1 and 3.3 nm, respectively.

The XPS was used as a primary tool to characterize the chemical composition of catalyst. The survey spectra (Fig. 9(a)) display a strong C 1s signal at ca. 286 eV together with Pd 3d signals at 334–342 eV and an O 1s signal at ca. 532 eV, while the existence of N in Pd/N-C-900 catalyst was not obviously. High-resolution spectra for C 1s and N 1s of Pd/N-C-900 catalyst were shown in Fig. 9(b) and (c), respectively. The C 1s results of XPS shown in Fig. 9(b) reveal the formation of various surface groups in the obtained composites. The spectra may be reasonably deconvoluted into four components corresponding to the following carbon functional groups: C–C (284 eV), C–N&C=O (285 eV), C–O (286.5 eV) and C=O (288.5 eV), respectively [39,40]. The N 1s spectrum was very useful for analyzing the nature of N functionalities. Four N-containing groups were possibly present in the catalyst from Fig. 9(c), which were pyridinic N (N1, 398.1 eV), amino N (N2, 399.6 eV), pyrolic N (N3, 400.5 eV) and graphitic N or quaternary N (N4, 403 eV) respectively [39]. The high resolution N 1s spectrum revealed pyridinic N (N1) and pyrolic N (N3) were the main nitrogen containing component of Pd/N-C-900 catalyst, which as discussed previously serves as the active site for anchoring the metal/alloy NPs [20,41–43]. According to the high-resolution spectra of Pd 3d for the Pd/N-C-900 catalysts (Fig. 9(d)), the peaks at 334.70 and 340.06 eV were ascribed to metallic Pd, while the peaks at 336.00 and 341.01 eV were assigned to Pd (II) species; for Pd/C-C catalyst (Fig. 9(e)), the peaks at 335.38 and 340.66 eV were ascribed to metallic Pd, while the peaks at 336.94 and 342.28 eV were assigned to Pd (II) species; for Pd/C catalyst (Fig. 9(f)), the peaks at 335.10 and 340.63 eV were ascribed

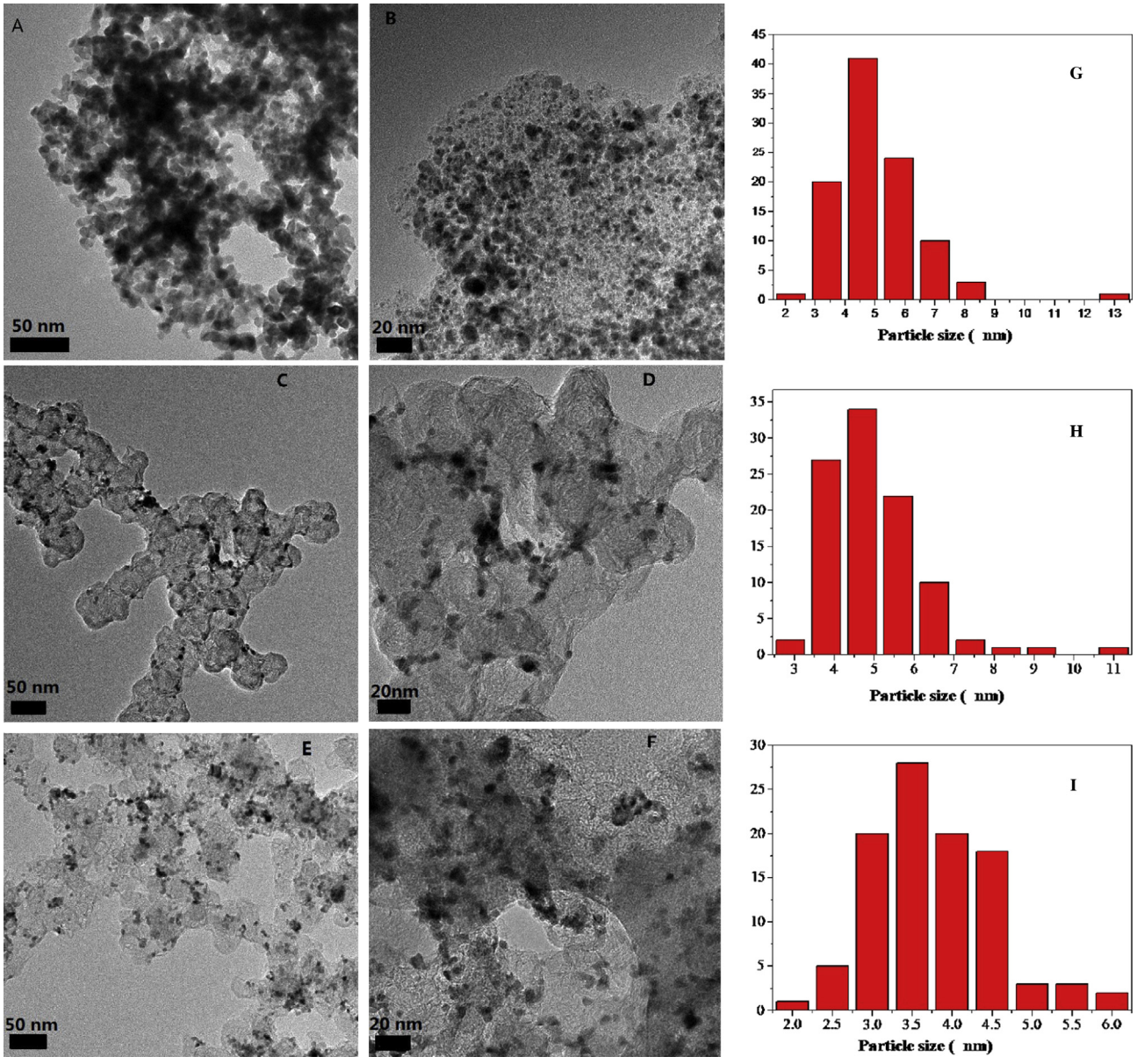

Fig. 10. TEM images of the catalysts and the corresponding particle size distribution histograms: Pd/C-C (A, B, G), Pd/C (C, D, H) and Pd/N-C-900 (E, F, I). The average particle size and corresponding size distributions were obtained by measuring the size of 100 randomly selected particles in the magnified TEM images.

to metallic Pd, while the peaks at 337.20 and 341.54 eV were assigned to Pd (II) species. It was evident that all the peaks of the binding energy for Pd/N-C-900 catalyst shifted towards the direction with lower binding energy values compared to the other two catalysts, indicating a strong interaction between the support and Pd. Meanwhile, the percentage composition of metallic Pd in Pd/N-C-900 and Pd/C catalysts was much higher than that in Pd/C-C catalyst, which was consistent with the above results of XRD, indicating that the commercial Pd/C-C catalyst contains more Pd oxides/hydrous oxides.

The TEM measurement was used to estimate the influence of the nitrogen on the morphology, the size and the dispersion of the Pd NPs. Fig. 10 shows the TEM images of the different catalysts and the corresponding particle size distribution histograms. Obviously, the aggregation of the Pd NPs in Pd/C-C catalyst was serious (consistent with Ref. [8]), while the dispersion of the Pd NPs in Pd/C catalyst was not uniform accompanying with some degree of aggregation; the dispersion of the Pd particles on Pd/N-C-900 was the best, which have a uniform size distribution over the entire range of the TEM image. The average particle size of Pd NPs in the Pd/C-C, Pd/C and Pd/N-C-900 catalysts was approximately 4.5, 4.6 and 3.5 nm, respectively. This result was consistent with the size calculated from the XRD data. The major size distribution of Pd NPs for Pd/C-C (Fig. 10G), Pd/C (Fig. 10H) and Pd/N-C-900 (Fig. 10I) was 3–7.5 nm, 3.5–7.5 nm and 2.75–4.75 nm, respectively. Hence, Pd NPs in the Pd/N-C-900 catalyst have the smallest size, narrowest size distribution compared with the Pd/C-C and Pd/C catalysts. The TEM measurement demonstrates that the addition of nitrogen into carbon support inhibited the aggregation of Pd particles, leading to smaller particle size, narrower size distribution as well as higher particle density in these systems. All these features agree well with that reported for the immobilization of NPs on N-doped carbon materials [44,45]. Accordingly, the nitrogen atoms in N-C have been proposed to act as localized defects that can make the acetylene carbon black chemically active for enhanced interactions with Pd NPs and hence facilitated their assembly and dispersion on the surface.

From the above results, the enhanced catalytic activity of Pd/N-C-900 for FAEO could be analyzed as follows. Firstly, the Pd NPs supported on the nitrogen doped acetylene carbon black substrate have smaller particle size compared to Pd NPs supported on the original acetylene carbon black. The smaller particle size leads to larger specific surface area, therefore provides more active sites at per unit mass of Pd for the oxidation reaction of formic acid. Secondly, improved dispersion, decreased Pd NPs agglomeration, higher Pd particle density can increase the amount of catalytic surface area accessible to the formic acid and electrolyte solution, thereby also improving the catalytic activity. Finally, the nitrogen containing functional groups in the catalyst can change the electron structure of the supported Pd catalysts by the interaction between support and catalyst. Hence, the electrocatalytic activity and stability for the Pd/N-C-900 catalyst were improved by synergetic effect of catalyst and support.

4. Conclusion

A series of Pd catalysts supported on nitrogen-doped acetylene carbon black (Pd/N-C-T catalyst) were successfully prepared by a very simple chemical reduction method. When the heat treatment temperature of support was 900 °C, the corresponding catalyst, Pd/N-C-900 catalyst possesses excellent catalytic activity and stability for FAEO. H_{ad} and CO_{ad} stripping voltammograms show that the Pd/N-C-900 catalyst has the largest ECSA and better tolerance of CO poisoning compared to homemade and commercial Pd/C catalyst. The peak current density of Pd/N-C-900 catalyst for FAEO was about 2.84 times higher than the undoped Pd/C catalyst and even about 0.96 times higher than commercial Pd/C catalyst. Furthermore, the enhanced catalytic activity on nitrogen-doped catalysts was confirmed in different formic acid concentrations and different experimental temperatures. XPS results indicated that there were four N-containing groups in the Pd/N-C-900 catalyst and the peaks binding energy of Pd for Pd/N-C-900 catalyst shifted towards the direction with lower binding energy values compared to undoped and commercial Pd/C catalyst. The average particle size of Pd NPs in the Pd/N-C-900 catalyst was about 3.5 nm with good dispersion and narrow size distribution. The enhanced performance was mainly attributed to the presence of nitrogen functional groups in the support which formed the strong support–catalysts interaction and large surface area. Due to the simple preparation method and superior electrocatalytic performance, the Pd/N-C-900 catalyst has great potential application for DFAFCs.

Acknowledgements

We are grateful for the financial support from the National Natural Science Foundation of China (20933004, 21073180, 21011130027), National Basic Research Program of China (973 Program, 2012CB215500, 2012CB932800). The Natural Science Foundation of Hebei Province (B2012203069) and Education Department of Hebei Province on Natural Science Research Key Projects for Institution of Higher Learning (ZH2011228) are also acknowledged.

References

[1] S. Uhm, H.J. Lee, J. Lee, Phys. Chem. Chem. Phys. 11 (2009) 9326–9336.
[2] C. Rice, S. Ha, R.I. Masel, P. Waszczuk, A. Wieckowski, T. Barnard, J. Power Sources 111 (2002) 83–89.
[3] C. Rice, S. Ha, R.I. Masel, A. Wieckowski, J. Power Sources 115 (2003) 229–235.
[4] Y. Zhu, Su Y. Ha, R.I. Masel, J. Power Sources 130 (2004) 8–14.
[5] X. Yu, P.G. Pickup, J. Power Sources 182 (2008) 124–132.
[6] Y.W. Rhee, S.Y. Ha, R.I. Masel, J. Power Sources 117 (2003) 35–38.
[7] N.V. Rees, R.G. Compton, J. Solid State Electrochem. 15 (2011) 2095–2100.
[8] R. Larsen, S. Ha, J. Zakzeski, R.I. Masel, J. Power Sources 157 (2006) 78–84.
[9] T. Maiyalagan, A.B.A. Nassr, T.O. Alaje, M. Bron, K. Scott, J. Power Sources 211 (2012) 147–153.
[10] C.W. Xu, H. Wang, P.K. Shen, S.P. Jiang, Adv. Mater. 19 (2007) 4256–4259.
[11] M. Arenz, V. Stamenkovic, T.J. Schmidt, K. Wandel, P.N. Ross, N.M. Markovic, Phys. Chem. Chem. Phys. 5 (2003) 4242–4251.
[12] X. Yu, P.G. Pickup, J. Power Sources 187 (2009) 493–499.
[13] X. Li, I.M. Hsing, Electrochim. Acta 51 (2006) 3477–3483.
[14] L. Feng, F. Si, S. Yao, W. Cai, W. Xing, C. Liu, Catal. Commun. 12 (2011) 772–775.
[15] S. Blaira, D. Lyckeb, C.A. Iordachec, ECS Trans. 3 (2006) 1325–1332.
[16] M. Ren, Y. Kang, W. He, Z. Zou, X. Xue, D.L. Akins, H. Yang, S. Feng, Appl. Catal. B Environ. 104 (2011) 49–53.
[17] T.T. Cheng, E.L. Gyenge, J. Appl. Electrochem. 39 (2009) 1925–1938.
[18] I.S. Park, K.W. Park, J.H. Choi, C.R. Park, Y.-E. Sung, Carbon 45 (2007) 28–33.
[19] B. Choi, H. Yoon, I.S. Park, J. Jang, Y.E. Sung, Carbon 45 (2007) 2496–2501.
[20] Y. Zhou, K. Neyerlin, T.S. Olson, S. Pylypenko, J. Bult, H.N. Dinh, T. Gennett, Z. Shao, R. O'Hayre, Energy Environ. Sci. 3 (2010) 1437–1446.
[21] Z. Lei, L. An, L. Dang, M. Zhao, J. Shi, S. Bai, Y. Cao, Microporous Mesoporous Mater. 119 (2009) 30–38.
[22] W.C. Fang, Nanoscale Res. Lett. 5 (2009) 68–73.
[23] Y. Ma, S. Jiang, G. Jian, H. Tao, L. Yu, X. Wang, X. Wang, J. Zhu, Z. Hu, Y. Chen, Energy Environ. Sci. 2 (2009) 224–229.
[24] B. Xiong, Y. Zhou, Y. Zhao, J. Wang, X. Chen, R. O'Hayre, Z. Shao, Carbon 52 (2012) 181–192.
[25] X. Zhao, J. Zhu, L. Liang, J. Liao, C. Liu, W. Xing, J. Mater. Chem. 22 (2012) 19718–19725.
[26] G. Bae, D.H. Youn, S. Han, J.S. Lee, Carbon 51 (2013) 274–281.
[27] H. Yoon, S. Ko, J. Jang, Chem. Commun. (2007) 1468–1470.
[28] L. Feng, S. Yao, X. Zhao, L. Yan, C. Liu, W. Xing, J. Power Sources 197 (2012) 38–43.
[29] A. Capon, R. Parsons, J. Electroanal. Chem. (1973) 205–231.
[30] T. Kawaguchi, W. Sugimoto, Y. Murakami, Y. Takasu, Electrochem. Commun. 6 (2004) 480–483.
[31] Y. Takasu, T. Fujiwara, Y. Murakami, K. Sasaki, M. Oguri, T. Asaki, W. Sugimoto, J. Electrochem. Soc. 147 (2000) 4421–4427.
[32] Y. Suo, I.M. Hsing, Electrochim. Acta 55 (2009) 210–217.

[33] M. Chen, Z.B. Wang, K. Zhou, Y.Y. Chu, Fuel Cells 10 (2010) 1171–1175.
[34] Y.W. Lee, J.K. Oh, H.S. Kim, J.K. Lee, S.B. Han, W. Choi, K.W. Park, J. Power Sources 195 (2010) 5896–5901.
[35] D. Morales-Acosta, J. Ledesma-Garcia, L.A. Godinez, H.G. Rodríguez, L. Álvarez-Contreras, L.G. Arriaga, J. Power Sources 195 (2010) 461–465.
[36] M. Sevilla, A.B. Fuertes, Carbon 44 (2006) 468–474.
[37] E. Antolini, F. Cardellini, J. Alloys Compd. 315 (2001) 118–122.
[38] V. Radmilovic, H.A. Gasteiger, P.N. Ross, J. Catal. 154 (1995) 98–106.
[39] Z. Lin, M. Song, Y. Ding, Y. Liu, M. Liu, C. Wong, Phys. Chem. Chem. Phys. 14 (2012) 3381–3387.
[40] K.R. Lee, K.U. Lee, J.W. Lee, B.T. Ahn, S.I. Woo, Electrochem. Commun. 12 (2010) 1052–1055.
[41] B.P. Vinayan, R. Nagar, N. Rajalakshmi, S. Ramaprabhu, Adv. Funct. Mater. 22 (2012) 3519–3526.
[42] S. Jiang, Y. Ma, G. Jian, H. Tao, X. Wang, Y. Fan, Y. Lu, Z. Hu, Y. Chen, Adv. Mater. 21 (2009) 4953–4956.
[43] G. Yang, Y. Li, R.K. Rana, J. Zhu, J. Mater. Chem. A 1 (2013) 1754–1762.
[44] R.I. Jafri, N. Rajalakshmi, S. Ramaprabhu, J. Mater. Chem. 20 (2010) 7114–7117.
[45] J. Zhang, J. Lei, R. Pan, Chuan Leng, Z. Hu, H. Ju, Chem. Commun. 47 (2011) 668–670.